JOURNAL OF MATERIALS SCIENCE **34** (1999) 2241–2251

Evaluating microstructural and damage effects in rule-of-mixtures predictions of the mechanical properties of Ni-Al_2O_3 composites

H. A. BRUCK, B. H. RABIN
Idaho National Engineering Laboratories, P.O. Box 1625, Idaho Falls, ID, 83415-2218, USA
E-mail: bhr@inel.gov

Ni-Al_2O_3 composites containing 0 to 100 vol % Ni were fabricated using powder processing techniques. By varying the metal : ceramic particle size ratio, either particle-reinforced or interpenetrating-phase microstructures were obtained. The mechanical properties of the composites were characterized and compared with rule-of-mixtures (ROM) predictions. For certain particle-reinforced composites, the elastic moduli measured ultrasonically did not obey the ROM. This result was attributed to the presence of damage that could be accounted for using existing models. In four-point bending, most composites exhibited linear elastic behavior, however significant inelastic deformation was observed for composites containing 60 and 80 vol % Ni. The inelastic deformation was reasonably well described using ROM models, except when substantial damage was present. Damaged materials were modeled as two phase composites containing one damage-free phase and one completely damaged phase that was assumed to behave like a porous material. The failure strains of composites with continuous ceramic phases were explained using a semi-empirical model that included both damage and residual stress effects. Fracture stresses were calculated from predicted fracture strains using a new ROM deformation model. The model was modified to include constraint effects in order to accurately describe the deformation behavior of the ductile continuous-ceramic composites.

1. Introduction

The mechanical properties of metal-ceramic composites represents an important field of study relevant to a wide variety of materials systems. One area of recent emphasis has been the study of functionally graded materials (FGMs), a new class of composites in which the microstructure and properties vary with position in the material. In these and other studies, the constitutive assumptions for composite materials are often critical to the success of modeling such phenomena as residual stresses and fracture behavior [1–4]. Although this originated out of research on FGMs, the results and modeling approaches presented herein are believed to be widely applicable.

A number of different modeling approaches can be used to describe the mechanical behavior of metal-ceramic composites. These approaches can be broadly categorized as being either macroscopic or microscopic in nature. Macroscopic models predict the average or global response of a composite using only the volume fraction and properties of the individual phases. These models are simplistic in that microstructural details such as the reinforcement size, shape, arrangement and orientation are ignored. Whether derived empirically or from continuum assumptions, these models usually give rise to the well known rule-of-mixtures (ROM) formulations [5]. By accounting in various ways for the interactions between the phases, the ROM estimates can be modified to include some microstructural details, e.g. the arrangement or degree of contact between the phases, often resulting in better agreement with experimental observations [6–11]. Regardless of the method used, these approaches rely upon the implicit assumption that the material is homogeneous on a macroscopic scale, i.e. the dimensions of the discrete microstructural constituents are small compared to the size scale over which the properties are measured.

Microscopic models typically use mean-field theories to estimate the overall deformation response of a composite by considering the behavior of the constituent phases. The most common method involves computing the average stress and strain fields for discrete particles isolated within a matrix phase using various forms of Eshelby's equivalent inclusion method [12–15]. In these models, microstructural details such as the amount, size, shape and orientation of the reinforcement can be explicitly taken into consideration, and good agreement with experiments has been observed in many cases. Alternatively, various FEM models have also been used to extensively investigate the effects of microstructural details on composite deformation response [16, 17]. FEM methods are

computationally intensive, but have the advantage of being able to readily incorporate plasticity and temperature dependent thermomechanical properties of the phases, which are difficult to include in other models.

Each of these modeling approaches has certain advantages and disadvantages. For example, although microscopic models offer the ability to include microstructural details, they have the disadvantage of being mathematically complicated and limited to discrete particle microstructures. Therefore, in spite of their obvious simplicity, ROM models are advantageous due to their ease of use and applicability to a wide range of microstructural types. The choice of which modeling method to use for a particular problem therefore depends upon the level of detail desired, convenience, and the degree of accuracy required.

In previously published FEM studies on residual stresses in Ni-Al_2O_3 FGM specimens, a modified ROM approach was adopted to estimate the properties of the composite materials that comprise the FGM interlayer [1, 2]. This empirical approach, originally proposed by Tamura *et al.* [10], involves distributing both the stresses and strains among the constituent phases in the composite according to their volume fractions and the slope of a line drawn between points on the stress-strain curve for each phase. The slope of the tie-line, q, determines the partitioning of stress and strain in the microstructure, with a vertical slope ($q = -\infty$) representing an isostrain condition and a horizontal slope ($q = 0$) representing an isostress condition. The value of the empirical q parameter depends upon many factors, including composition, flow stress ratio and strain hardening of the constituent phases, their microstructural arrangement, and the applied strain. The exact nature of this dependence, however, is not well known. Fischmeister and Karlsson [11] experimentally determined that a slope of $q = -4.5$ GPa yielded useful results for a variety of two phase materials containing hard and soft constituents that were studied over a range of volume fractions and applied strains.

In order to justify use of the modified ROM described above, experimental verification of the accuracy of the ROM estimates has been sought. In this study, the powder processed Ni-Al_2O_3 composites were produced in bulk form. Composites were fabricated for a range of compositions between pure metal and pure ceramic using two different ceramic : metal particle size ratios, yielding a variety of particle-reinforced and interpenetrating-phase microstructures. The elastic modulus and deformation behavior of each composite were measured using ultrasonic and four-point bending methods. These results were compared with the modified ROM model described above, as well as with a ROM-based model developed by Ravichandran for particle-reinforced and interpenetrating-phase metal-ceramic composites [6, 7]. Ravichandran used a ROM formulation at the microstructural level, and included the effects of constraint, to predict deformation results similar to the numerically intensive micromechanical and FEM methods. In this study, significant disagreement between the experimental results and the ROM models was attributed to the presence of damage in the composites. Existing models incorporating the effects of damage were used to explain the elastic moduli results [18, 19]. It was determined that Ravichandran's formulation could be applied to predict the deformation behavior of the damaged composites by modeling them as a two-phase mixture consisting of one damage-free composite phase and one completely damaged porous phase.

Although models exist for predicting the deformation behavior of these composites, models do not exist for predicting their failure. In this study, the tensile failure strains of continuous-ceramic composites containing 20 to 100 vol % Ni were predicted using a new semi-empirical model. This model was developed by incorporating the effects of thermal residual stresses into the empirical relationship between mechanical properties and porosity described by Coble and Kingery for Al_2O_3 [20]. Fracture stresses were predicted from the fracture strains using a new and simple deformation model developed by incorporating Coble and Kingery's empirical relationship for the deformation behavior of porous Al_2O_3 into a ROM formulation.

2. Experimental procedure

Homogeneous bulk composite specimens approximately 25 mm × 25 mm × 75 mm were prepared using the powder processing techniques described elsewhere [21]. The Ni and Al_2O_3 powders were mixed, compacted, pre-sintered, and then consolidated in a hot isostatic press (HIP) at 1350 °C. Specimens were fabricated from powder compacts having nominal compositions of 0, 5, 10, 20, 40, 60, 80, and 100 vol % Ni. Two different combinations of powder sizes were used, either 5 μm Ni with 22 μm Al_2O_3 or 18 μm Ni with 0.5 μm Al_2O_3, respectively. The submicron Al_2O_3 powder, along with Mn and Ti sintering aids, was required to obtain substantial densification and interparticle bonding in composites containing a continuous ceramic phase. In the case of the 5 μm Ni and 22 μm Al_2O_3 samples, compositions with less than 40 vol % Ni where poorly bonded and were not studied.

Portions of each specimen were removed for ultrasonic measurements, and the remaining portions were machined into rectangular test bars having dimensions 50 mm × 4 mm × 3 mm. Mechanical tests were conducted on the rectangular bars in an Instron load frame using a four-point bend configuration with an upper span of 40 mm and a lower span of 20 mm. Strains were calculated from crosshead displacements, as well as measured directly using strain gages. All specimens were loaded to failure, except for the 60 and 80 vol % Ni compositions produced from the 5 μm Ni with 22 μm Al_2O_3 for which the inelastic deformation exceeded approximately 2%. Load-displacement were used to calculate stresses and strains as described below.

For elastic-plastic deformations, the applied bending moment, M, can be related to the strain on the outer fiber of the bend bar, ε, using the following well known formula:

$$\frac{M}{M_0} = \frac{-n+1}{2n+1}\left(\frac{\varepsilon_0}{\varepsilon}\right)^2 + \frac{3n}{2n+1}\left(\frac{\varepsilon}{\varepsilon_0}\right)^{\frac{1}{n}} \quad (1)$$

where M_0 is the bending moment at yielding and ε_0 is the tensile yield strain for the outer fiber. This equation is derived assuming the yield behavior in tension and compression are identical and that the material obeys a power hardening law as follows:

$$\frac{\sigma}{\sigma_0} = \begin{cases} \varepsilon/\varepsilon_0 & \text{for } |\varepsilon| \leq \varepsilon_0 \\ (\varepsilon/\varepsilon_0)^{\frac{1}{n}-1}\varepsilon/\varepsilon_0 & \text{for } |\varepsilon| > \varepsilon_0 \end{cases} \quad (2)$$

where σ_0 is the yield stress, ε_0 is the yield strain, and n is the strain hardening exponent.

The outer fiber elastic strain, ε, was measured indirectly from the radius of curvature of the bar, r_c, as follows:

$$\varepsilon = \frac{h}{2r_c} \quad (3)$$

The radius of curvature was calculated from the crosshead displacement of the upper fixture, Δ, as follows:

$$r_c = \frac{L^2}{12\Delta} \quad (4)$$

where L is the lower span of the four-point bend fixture. The displacement of the crosshead includes displacements due to the compliance of the test fixture. It was possible to account for this contribution by comparing the Young's moduli from the four-point bend measurements with ultrasonic measurements for a purely elastic material such as Al_2O_3.

3. Results

3.1. Microstructural analysis

In order to model the deformation behavior of the Ni-Al_2O_3 composites, it was first necessary to characterize the microstructures. Density measurements performed using the immersion method indicated that all samples were consolidated to greater that 99% of theoretical density. Optical micrographs showing the microstructures of composites produced from the 5 μm Ni and 22 μm Al_2O_3 powders can be seen in Fig. 1a, and those produced from the 18 μm Ni and 0.5 μm Al_2O_3 can be seen in Fig. 1b. The apparent porosity evident in these figures is due to particle pullout during metallographic preparation. Composites fabricated from 5 μm Ni and 22 μm Al_2O_3 powders exhibited microstructures consisting of a continuous Ni matrix reinforced with discrete Al_2O_3 particles; however, at the lowest Ni content (40 vol % Ni) there was considerable contact and contiguity between the Al_2O_3 particles, and it is difficult to discern if the Al_2O_3 phase forms an interconnected network. Composites fabricated from 18 μm Ni and 0.5 μm Al_2O_3 powders exhibited microstructures consisting essentially of a continuous Al_2O_3 matrix reinforced with discrete Ni particles, except for the highest Ni content (80 vol % Ni) which appears to also have an interconnected Ni phase. Since, in some cases, it is impossible to determine from a micrograph taken from the cross-section of a composite whether the reinforcement exists as discrete particles (or discrete agglomerates) or as an interconnected phase, further analysis was required.

Percolation theory [22] states that the transition from a discrete particle microstructure to a microstructure exhibiting long-range connectivity occurs at a critical value of the volume fraction known as the percolation threshold. For metal-ceramic composites, the percolation threshold for the conductive (metal) phase, V_{cr}, can be determined experimentally from resistivity measurements using the following relationship between

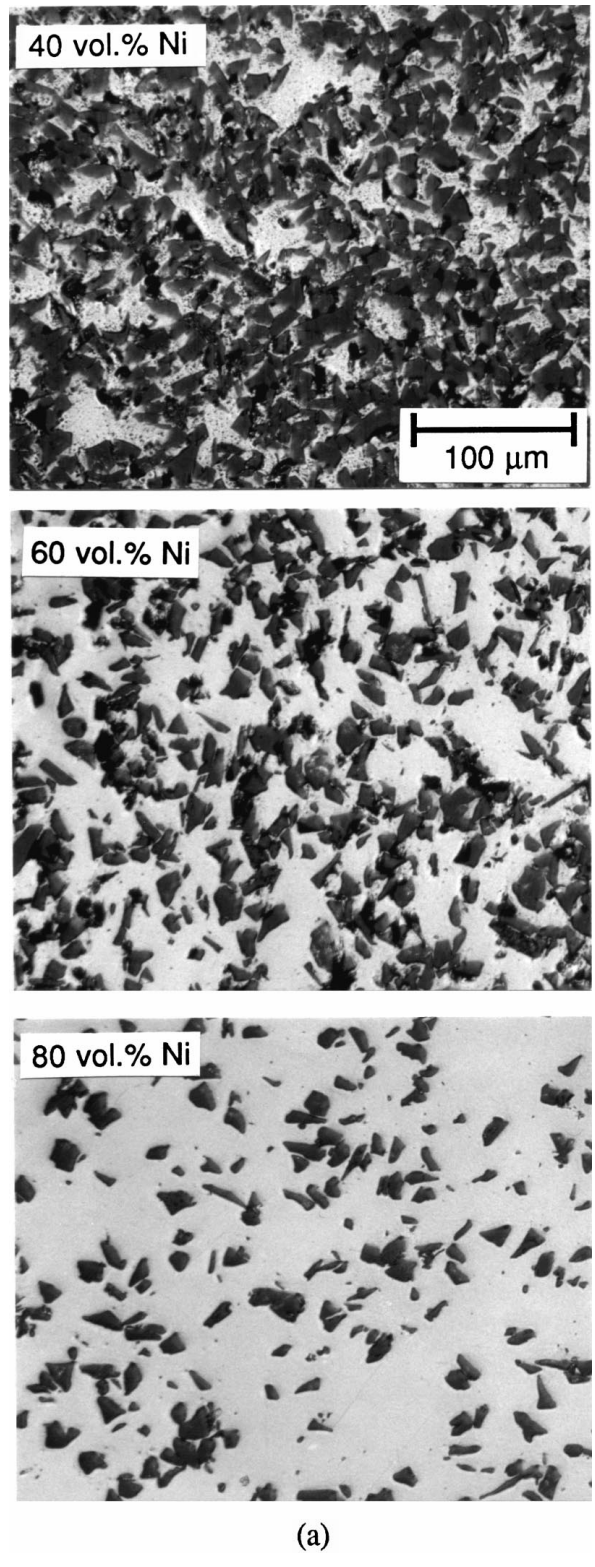

Figure 1 Optical micrographs showing the microstructures of composites fabricated from (a) 5 μm Ni and 22 μm Al_2O_3 powders and (b) 18 μm Ni and 0.5 μm Al_2O_3 powders.

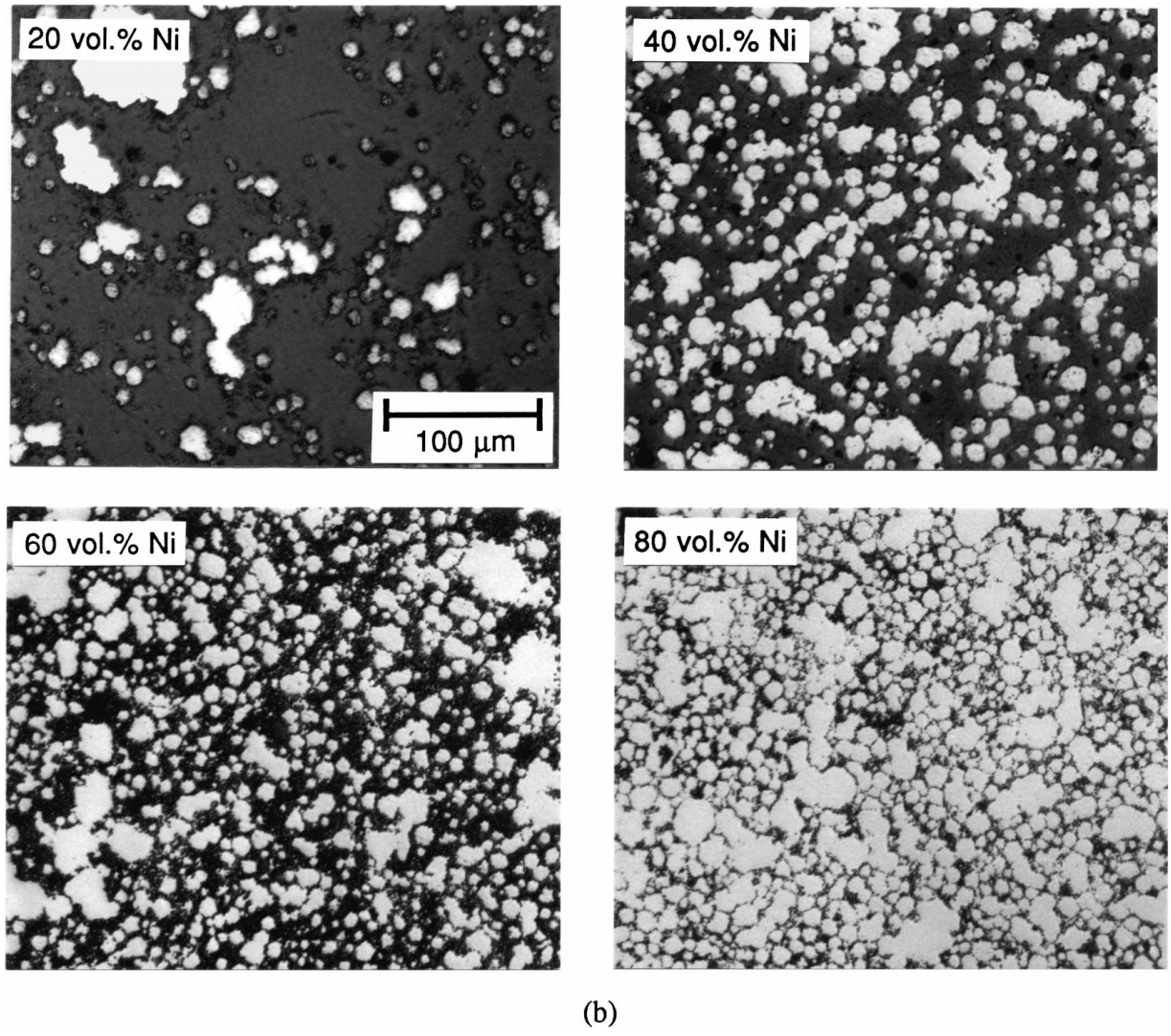

Figure 1 (*Continued*).

resistivity, R, and volume fraction:

$$R \propto (V_m - V_{cr})^{-2} \quad (5)$$

where V_m is the volume fraction of metal. Resistivity measurements for the composites are shown in Fig. 2. The percolation thresholds for the Ni phase estimated from the above analysis are $V_{cr} = 0.10$ for composites fabricated from the 5 μm Ni and 22 μm Al_2O_3 powders and $V_{cr} = 0.30$ for composites fabricated from the 18 μm Ni and 0.5 μm Al_2O_3 powders. Thus, composites produced from the 5 μm Ni and 22 μm Al_2O_3 powders (which all contained 40 vol % Ni or greater) can all be characterized as having a continuous Ni phase, as suggested in Fig. 1a. Composites produced from the 18 μm Ni and 0.5 μm Al_2O_3 powders can be characterized as having discrete Ni particles for Ni concentrations of 20 vol % or less, and are characterized as having a connected Ni phase for Ni concentrations of 40 vol % or greater. Unfortunately, no direct measurement was possible to allow the percolation threshold for the Al_2O_3 phase to be characterized. For the purposes of the present analysis, the 5 μm Ni and 22 μm Al_2O_3 composite containing 40 vol % Ni was assumed to consist of a continuous Ni matrix with dispersed Al_2O_3 particles. Based on the resistivity measurements and the connectivity of the Al_2O_3 phase observed metallographically, the 18 μm Ni and 0.5 μm Al_2O_3 specimen containing 40 vol % Ni was determined to consist of interpenetrating phases. However, because this microstructure is near the percolation threshold for Ni, some Ni may still exist as discrete particles.

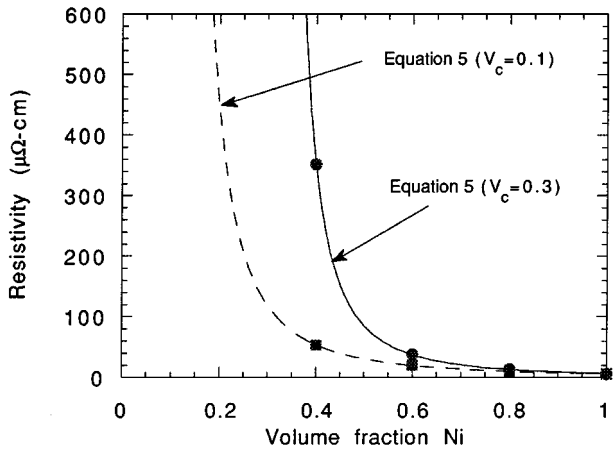

Figure 2 Resistivity measurements for Ni-Al_2O_3 composites.

In the analysis of the mechanical response of these materials presented in the following sections, a distinction is made between those microstructures that contain discrete reinforcement particles (which could be contained in either continuous metal matrix or continuous

TABLE I Microstructural types based on metallography and resistivity measurements

Composition (vol. % Ni)	Powder mixture: 5 μm Ni and 22 μm Al_2O_3	Powder mixture: 18 μm Ni and 0.5 μm Al_2O_3
5	Not studied	3
10	Not studied	3
20	Not studied	3
40	1*	2*
60	1	2
80	1	2

Key:
1 = continuous Ni matrix, dispersed Al_2O_3 particles
2 = interpenetrating phases
3 = continuous Al_2O_3 matrix, dispersed Ni particles
* see text for discussion.

ceramic matrix) and those that contain interpenetrating phases. Table I summarizes the microstructure characterization results with regard to this distinction, and also indicates the two composites for which the type of microstructure could not be unambiguously identified. The discussion regarding microstructures that exhibit continuous ceramic phases involves all composites produced from the 18 μm Ni and 0.5 μm Al_2O_3 powders and, as indicated in Table I, includes both types of microstructures.

The grain size within the Ni phase in the composites was measured to be in the range of 20 to 50 μm for all composites. In contrast, due to extensive grain growth the grain size for the pure Ni sample was on the order of 1 mm. It was not the focus of this work to manufacture pure Ni specimens having grain sizes comparable to those of the composites; however in order to be consistent with the grain size of the matrix in the composites the deformation behavior corresponding to fine-grained Ni was used in the following analyses. The power law hardening deformation response of the fine-grained Ni, obtained from the literature [23] was assumed to be:

$$\sigma(\text{GPa}) = 0.68\varepsilon^{0.25} \tag{6}$$

3.2. Ultrasonic measurements of elastic constants

3.2.1. Comparison with ROM predictions

Young's moduli were determined from ultrasonic measurements and the results are presented in Fig. 3 according to the type of composite microstructure (as identified in Table I). Fig. 3a shows results for all interpenetrating phase composites and 3b shows results for all of the particle-reinforced composites. Comparisons were made with predictions from the modified ROM model, Ravichandran's ROM model, and an additional model incorporating porosity that will be discussed below. In the case of the interpenetrating phase composites (Fig. 3a) note that the modified ROM and Ravichandran's predictions yield quite similar results, and both models are in excellent agreement with the experimental data for composites containing 60 and 80 vol % Ni. For the 40 vol % Ni composite the modulus is considerably lower than the ROM predictions. In

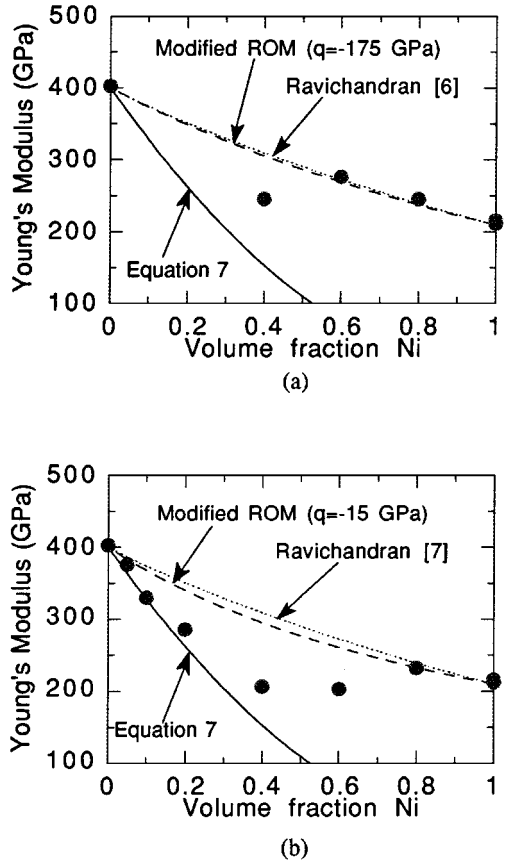

Figure 3 Ultrasonic measurements of Young's moduli for (a) particle-reinforced and (b) interpenetrating-phase Ni-Al_2O_3 composites.

the case of the particle-reinforced composites (Fig. 3b) only the 80 vol % Ni composite is in reasonable agreement with the model predictions, and all other moduli were lower than expected. The reasons for this disagreement are discussed below.

3.2.2. Influence of damage on composite modulus

It was suspected that the low moduli values for these composites could be attributed to damage in the form of either debonding between the Ni and Al_2O_3 phases, poor sinter bonding between contiguous 22 μm Al_2O_3 particles or particle fracture, although no direct evidence for the later was observed. To establish a lower bound on the expected modulus values in the damaged materials, it was initially assumed all the damage could be treated as porosity, and the empirical correlation presented by Coble and Kingery was used to relate the elastic modulus, E, to the amount of porosity present in the material, as follows [20]:

$$E = E_0(1 - 1.9\rho + 0.9\rho^2) \tag{7}$$

where ρ is the porosity and E_0 is the Young's modulus of the completely dense ceramic. The curves shown in Fig. 3 were calculated assuming all the reinforcement phase was porosity. Note that all modulus data fell between the ROM predictions and the porosity calculation, suggesting that this approach does indeed establish a useful lower bound. For the particle-reinforced composites containing less than 20 vol % Ni, excellent agreement was observed between the measured values

and the porosity prediction. This result suggests that there was essentially complete particle debonding in these materials.

In order to analyze the data for the composites with modulus values lying between the ROM and the completely damaged (porosity) bounds, a damage model was needed that incorporated varying degrees of damage. Models developed by Mochida *et al.* [18] can predict the reduction in the elastic moduli of the composite by treating the damaged particles as an additional particulate phase characterized by shattering, debonding or cracking. Tong and Ravichandran [19] utilized these models to predict the reduction in the elastic moduli of shock-consolidated SiC-particle-reinforced titanium-matrix composites, however the volume fraction of damaged SiC particles observed microscopically did not correlate with the model predictions; the discrepancy was attributed to microcracking in large particles that could not be observed microscopically.

Bulk modulus is insensitive to the type of damage present and is therefore appropriate for quantifying the amount of damage. The measured bulk moduli for the 40, 60, and 80 vol % Ni particle-reinforced microstructures were plotted with the damage model predictions (Fig. 4). For the 60 vol % Ni composite, the amount of damage corresponded to approximately 36% of the particles, while for the 40 vol % Ni composite approximately 30% of the particles were damaged. The 80 vol % Ni composite had significantly less damage, only 13%.

To evaluate the type of damage present, the measured elastic moduli for each these composites were compared with the predictions for the different damage types (Fig. 5). In all cases the analyses indicated the type of damage most closely corresponded to debonded particles. This observation is consistent with the damage types observed in Tong's composites [19]. However, it is believed that the local stress and strain states corresponding to debonded particles in the damage model are also reasonable for describing those in poorly sintered contiguous 22 μm Al_2O_3 particles.

Applying these damage models to the ultrasonic modulus data for the 0 to 20 vol % Ni particle-reinforced composites provides details on the quantity and type of damage. The quantity of damage was estimated to be 62% for the 5 vol % Ni composite, and 86 % for both the 10 and 20 vol % Ni composites. The damage appeared to be consistent with a mixture of debonded and shattered particles. This result is not unexpected since completely debonded particles would be expected to produce stress and strain states comparable to those for shattered particles, yet some particles are probably only partially debonded. The large quantity of damage in these composites explains the good agreement that was observed between the measured modulus values and the predictions based on Coble and Kingery's porosity correlation.

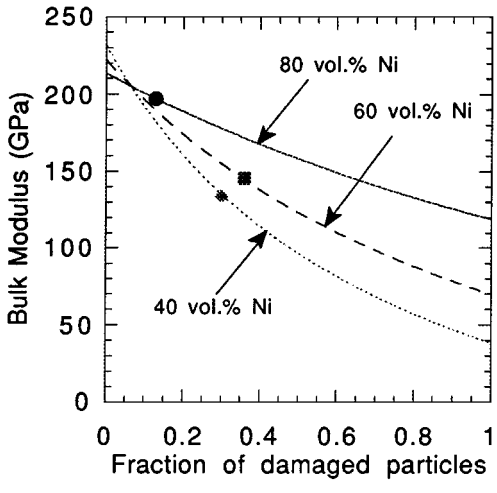

Figure 4 Bulk moduli for 40, 60 and 80 vol % Ni particle-reinforced composites measured using ultrasonics compared with predictions from the damage model proposed by Tong and Ravichandran [19].

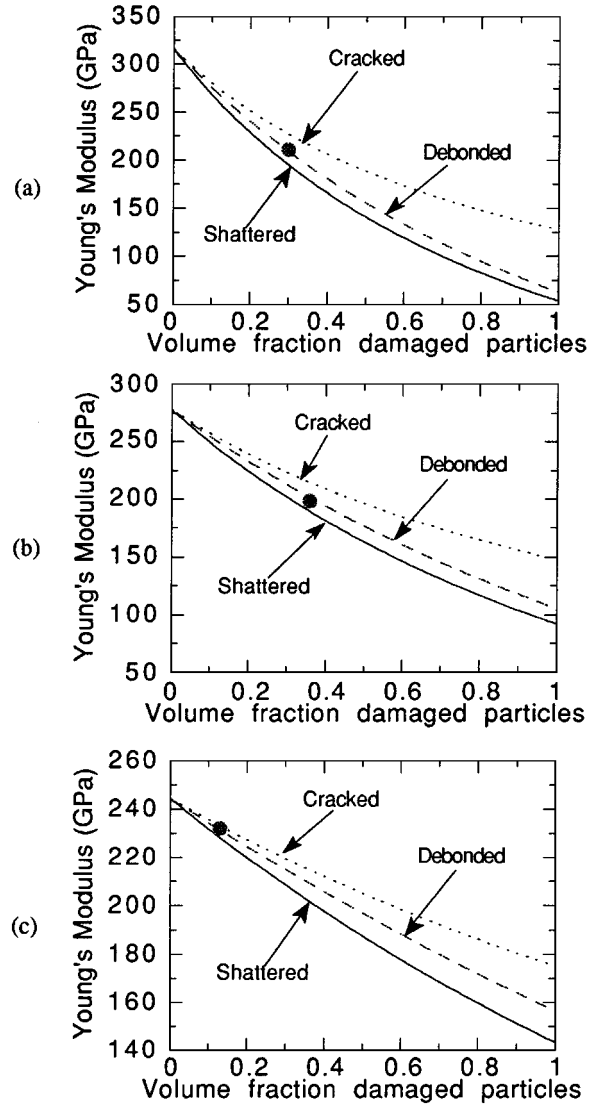

Figure 5 Young's modulus for the (a) 40 vol % Ni, (b) 60 vol % Ni, and (c) 80 vol % Ni particle-reinforced composites compared with the predictions for various assumed types of damage using the model of Mochida *et al.* [18].

3.3. Deformation behavior of ductile composites

3.3.1. Validation of assumption in four-point bend analysis

In order to verify the assumption that the composite yield behavior was identical in tension and compression, and consequently that the strains calculated using

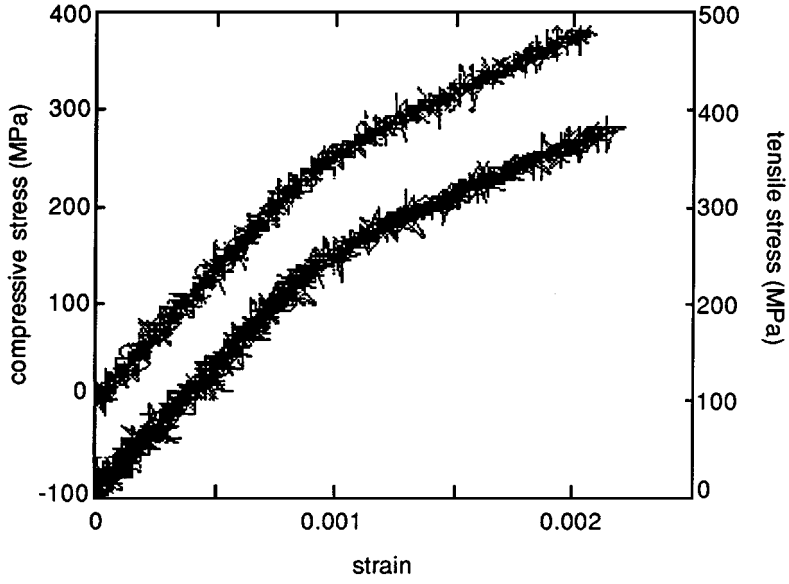

Figure 6 Strain gage measurements of tensile and compressive strains from a four-point bend test conducted on a 60 vol % Ni interpenetrating-phase composite.

crosshead displacements were accurate, strain gages were placed on the tensile and compressive sides of a 60 vol % Ni interpenetrating-phase composite. The measured strains, shown in Fig. 6, indicate that the yield behavior was nearly identical. This conclusion is consistent with the numerical modeling of Daehn *et al.* [24] indicating that thermal residual stresses cause only a slight difference between the compressive and tensile yield behavior for interpenetrating-phase composites. Shen *et al.* [16] also used numerical modeling to show that thermal residual stresses have the same effect on the yield behavior of composites with unit cylinder and spherical particle reinforcements as on the interpenetrating-phase composites. Based on these results, the assumption used in Equations 1 and 4 was justified.

3.3.2. Comparisons with ROM models

Measurements of the inelastic deformation in the ductile 60 and 80 vol % Ni composites were compared with the ROM models. The results for the interpenetrating-phase microstructure and particle-reinforced microstructure can be seen in Figs 7a and b, respectively.

The modified ROM model and the ROM model of Ravichandran [7] both provide adequate predictions of the deformation behavior for all but the 60 vol % Ni particle-reinforced composite. The values of q (slope of the tie-line in the modified ROM model) used in the analyses are also indicated on the figures. The behavior of the particle-reinforced composite approaches an isostress condition ($q = 0$ GPa) while that of the interpenetrating phase composite approaches an isostrain condition ($q = -\infty$ GPa). The model of Ravichandran appears to more accurately predict the deformation behavior.

3.3.3. Deformation modeling of damaged composites

The discrepancies between the ROM predictions and the observed deformation response for the 60 vol % Ni particle-reinforced composite are not surprising in light of the damage present in this material. In order to predict the deformation behavior of this material, it is therefore necessary to take damage into account in the constitutive models. The model of Ravichandran

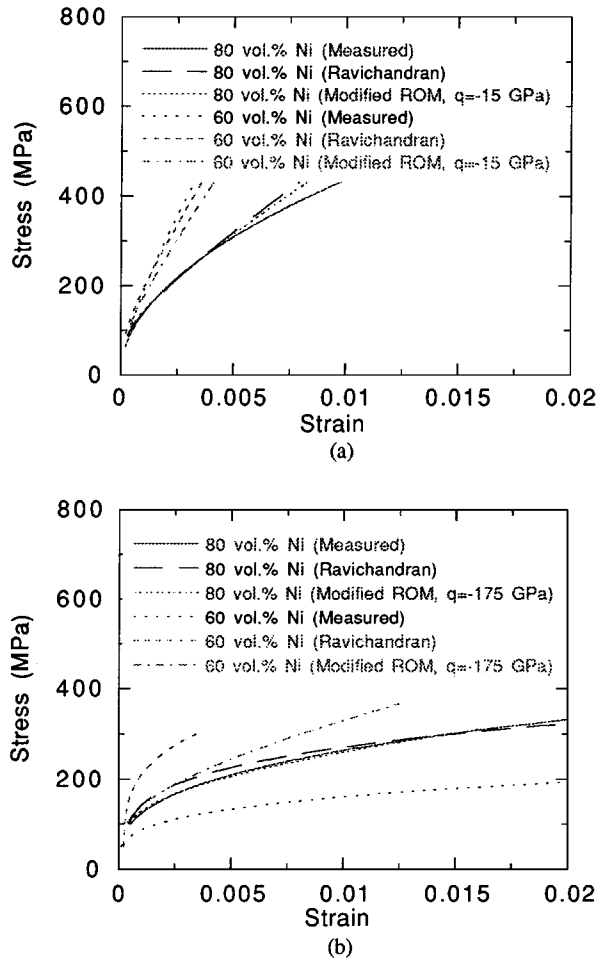

Figure 7 Deformation behavior of (a) interpenetrating-phase and (b) particle-reinforced Ni-Al_2O_3 composites compared with predictions made using the modified ROM and Ravichandran's models [6, 7].

can be utilized by treating the composite as two different particle-reinforced phases, one with completely damaged particles and one with completely undamaged particles.

The volume fraction of the completely damaged phase was assumed to be the same as the volume fraction of damaged particles determined from analysis of the elastic modulus data. Unfortunately, the deformation response of this completely damaged phase is not known. For the purpose of this analysis, it was assumed that the damaged phase could be treated as a porous metal with a porosity equal to the volume fraction of the particle reinforcement. From German [25], it is known that porosity, ρ, reduces the work hardening exponent of steel as follows:

$$n = 0.31(1 - \rho)^{-1.9} \tag{8}$$

In order to apply this relationship to Ni, the initial value of the work hardening exponent was taken to be 0.25 (from Equation 6) instead of 0.31. The modified work hardening exponent was used in conjunction with Equation 6 to represent the deformation behavior of the damaged Ni phase.

The deformation responses of the damaged composites predicted using Ravichandran's models for both interpenetrating-phase and particle-reinforced composites are shown in Fig. 8. The damaged interpenetrating-phase composite model better describes the deformation response of the of the 60 vol % Ni particle-reinforced composite (Fig. 8a). Predictions are also shown for the case in which the effects of constraint have been eliminated from the model, giving slightly better agreement with the observed behavior. This modification to the model for its application to damaged composites is justified since the completely damaged phase is highly compliant and cannot provide significant constraint on the undamaged phase.

The effects of damage in the 80 vol % Ni specimen are shown in Fig. 8b. Since this material contained only approximately 13% damage, the effects of accounting for this damage on the deformation behavior predicted using both composite models were relatively minor.

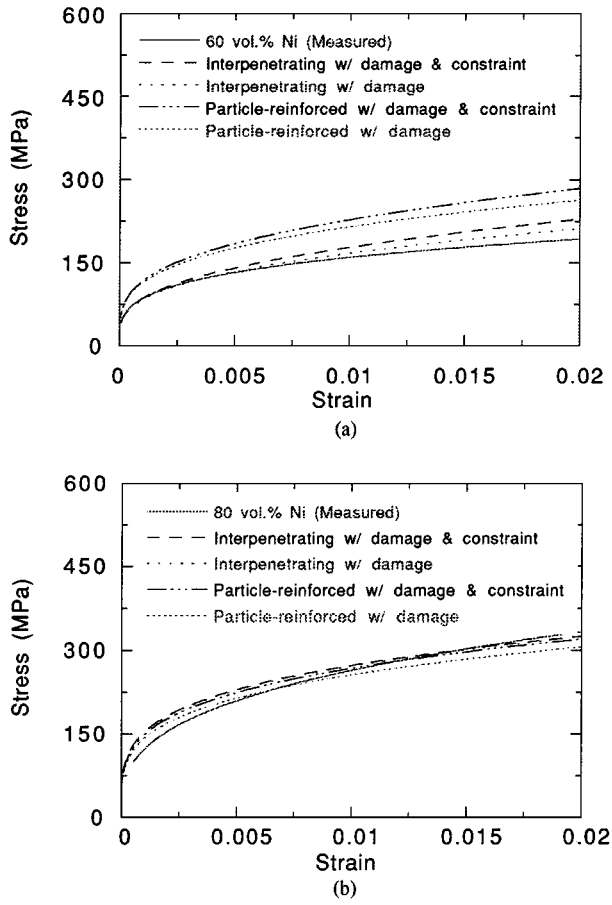

Figure 8 Predictions of the deformation behavior of damaged (a) 60 vol % Ni and (b) 80 vol % Ni particle-reinforced composites made using Ravichandran's interpenetrating-phase and particulate reinforced models, with and without constraint [6, 7].

3.4. Fracture of continuous ceramic-phase composites

3.4.1. Prediction of fracture strains

Almost all of the composites studied failed in a brittle manner, exhibiting relatively low fracture strains (i.e., less than 2%). However, the 80 vol % Ni particle-reinforced composite did not fail after 2% strain, at which point the four-point bend test was terminated. In the following analyses, fracture of the continuous ceramic-phase composites is described. Fracture strains and stresses for these materials having compositions ranging from 0 to 80 vol % Ni are shown in Figs 9a and b, respectively.

The following simple model was proposed to describe the fracture strain of these composites. The composites were assumed to be comprised of a continuous, porous ceramic phase penetrated with metal. Since the ceramic phase is continuous, the strain in the ceramic was assumed to be equal to the overall composite strain. It is further assumed that fracture of the brittle ceramic phase dictated failure of the composite. The fracture strain, ε_f, for a porous composite was calculated from the properties of porous Al_2O_3 [20] as follows:

$$\varepsilon_f = \frac{\sigma_f}{E} = \frac{-(\sigma_0/5)(1-\rho)\ln(0.6\rho)}{E_0(1 - 1.9\rho + 0.9\rho^2)} \tag{9}$$

where σ_f is the fracture stress, E is the Young's modulus, σ_0 is the fully dense fracture strength, and E_0 is the fully dense Young's modulus.

To apply Equation 9 to the continuous ceramic-phase composites, interactions between the ceramic and the reinforcement must be accounted for. During fabrication, residual stresses are developed in the ceramic and the metal due to the mismatch in thermal expansion coefficients. In the simplest case the interaction effect is equal to the residual stress. This is analogous to the treatment of hydraulic fracturing of rocks, wherein pore pressure has the effect of decreasing the fracture strength by an amount equal to the pressure [26]. This effect is described by the Griffith theory for a crack with internal pressure [27], and is valid for both positive and negative pressures. Thus, it is reasonable to assume for particle-reinforced ceramics that the thermal residual stresses, σ_{trs}, in the particulate phase will have an effect equivalent to that of pore pressure. Equation 9 can

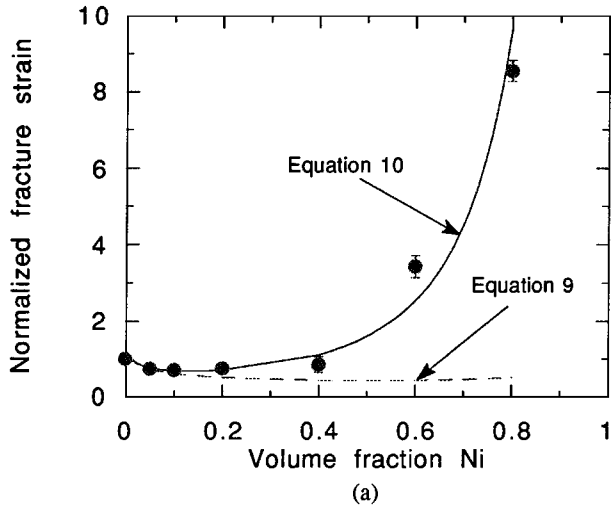

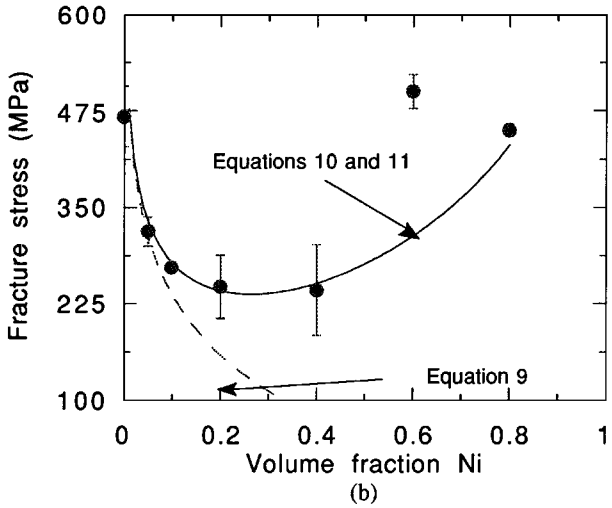

Figure 9 Measured and predicted fracture strains (a) and fracture stresses (b) for continuous ceramic-phase composites shown as a function of Ni content.

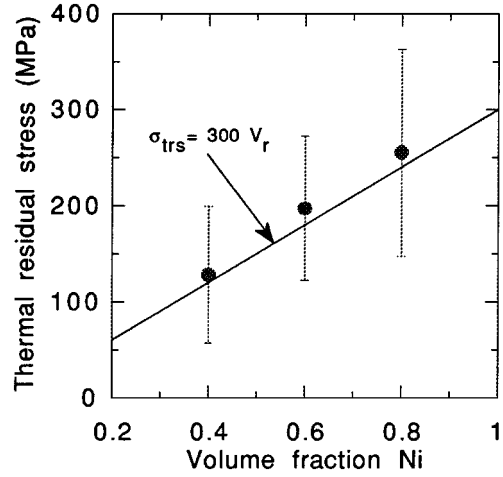

Figure 10 Thermal residual stresses measured using neutron diffraction techniques for interpenetrating-phase Ni-Al_2O_3 composites.

therefore be modified as follows:

$$\varepsilon_f = \frac{-(\sigma_0/5)(1-V_r)\ln(0.6V_r) + \sigma_{trs}}{E_0\left(1-1.9V_r+0.9V_r^2\right)} \qquad (10)$$

where the porosity of the ceramic has been replaced by the volume fraction of reinforcement, V_r. Although not done for this study, a more exact relationship between the thermal residual stresses and pore pressure could be determined for particle-reinforced composites using a micromechanical analysis based on Eshelby's equivalent inclusion model [28, 29]. Exact models are not currently available for composites with interpenetrating phases.

While it is reasonable to assume that the thermal residual stress in the particulate phase is equivalent to the pore pressure for particle-reinforced composites, this assumption may not be valid for interpenetrating-phase composites. In this case, the effect of the reinforcing phase is to pre-stress the ceramic by an amount equal to the thermal residual stress in the ceramic phase. For the present analysis it was assumed that the effects of pre-stressing are identical to the effects of pore pressure, so Equation 10 can also be applied to interpenetrating-phase microstructures by using the thermal residual stress in the ceramic rather than in a particle.

The thermal residual stresses in these materials have been determined experimentally using neutron diffraction measurements [30]. The results for the hydrostatic stress are shown in Fig. 10 as a function of Ni volume fraction. Note that the hydrostatic stresses in the ceramic increase almost linearly with Ni content in the range of 40 to 80 vol % Ni. However, for composites containing less than 40 vol % Ni, the residual stresses in the particles were negligible. These observations are consistent with the elastic modulus measurements that indicated substantial particle debonding for composites containing 20% Ni or less. Including the measured residual hydrostatic stresses in Equation 10 yields predictions of the fracture strain in good correlation with the measured values (Fig. 9a).

3.4.2. Prediction of fracture stresses

Fracture stresses can also be calculated from the fracture strains predicted in the previous section provided appropriate deformation models are used. As has been demonstrated, no single model can be used to predict the deformation behavior of these materials since some composites exhibit interpenetrating phases and some exhibit particle-reinforced microstructures. In the case of the continuous ceramic-phase composites, the deformation behavior was predicted using an empirical porous ceramic approach, identical to the formulation of Equation 9. Assuming no interaction between the ceramic and the reinforcing phase, the deformation behavior of the composite can be predicted from the deformation behavior of each phase using a simple ROM:

$$\sigma_{composite} = E_0\left(1-1.9V_r+0.9V_r^2\right)\varepsilon_{composite} + V_r\sigma_r(\varepsilon_{composite}) \qquad (11)$$

where $\sigma_{composite}$ is the composite stress and $\sigma_r(\varepsilon_{composite})$ is the deformation behavior of the reinforcing phase.

Fracture stresses calculated with Equation 11 using the predicted fracture strains (including the effect of residual stresses) are shown in Fig. 9b. In these

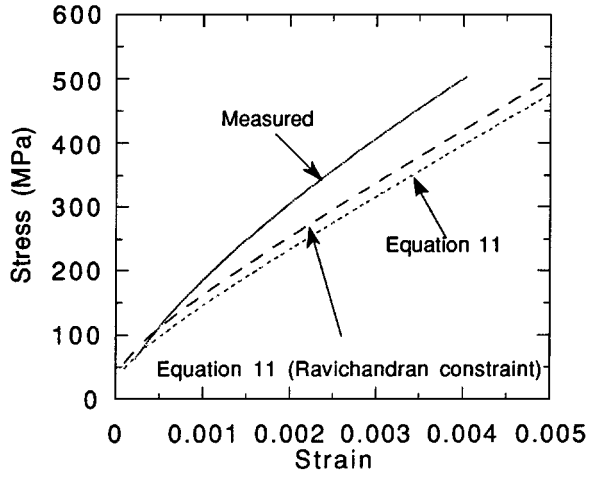

Figure 11 Deformation behavior of a 60 vol % Ni interpenetrating-phase composite compared with predictions made using Equation 11, with and without the constraint factor of Ravichandran [6].

calculations, the contribution of the Ni phase to the deformation behavior of the composites was neglected for materials containing 20 vol % Ni or less because of the substantial particle debonding previously demonstrated in these materials. Note that in the case of the 60 vol % Ni specimen, the model predicts a significantly lower fracture stress than would be expected based on the good agreement between the measured and predicted fracture strains (Fig. 9a). The reason for this disagreement is illustrated in Fig. 11 where the actual deformation behavior of the 60 vol % Ni specimen is compared with that predicted using Equation 11. The specimen was considerably less compliant than the model predicts. This effect was believed to be due to constrained deformation of the metal phase, therefore the calculations were repeated including the constraint parameter proposed by Ravichandran [6]. The modification, also shown in Fig. 11, had a relatively minor effect on the behavior predicted by Equation 11.

Elastic moduli predicted by Equation 11 are compared with predictions from Ravichandran's model for interpenetrating-phases in Fig. 12. Equation 11 predicts modulus values significantly lower, most notably near the 60 vol % Ni composition. Assuming this result is due to an interaction between the phases not accounted for in Equation 11, the model was modified to include a new constraint factor, $\phi(V_r)$, dependent upon the volume fraction of the Ni phase. Consequently, Equation 11 was rewritten as:

$$\phi(V_r)\sigma_{composite} = E_0\left(1 - 1.9V_r + 0.9V_r^2\right)\varepsilon_{composite} + V_r\sigma_r(\varepsilon_{composite}) \quad (12)$$

The new constraint factor can be evaluated by calculating the stresses in a hypothetical composite consisting of a reinforcing phase with the same properties as the ceramic phase. Since, in order to be self-consistent, the modulus of the composite must equal the modulus of the single phase material for all reinforcement volume fractions, the constraint factor must be of the form:

$$\phi(V_r) = 1 - 1.9V_r + 0.9V_r^2 \quad (13)$$

Using this constraint factor the moduli were again calculated and compared with the model of Ravichandran. As shown in Fig. 12, substantial agreement was obtained between the two models. In addition, the predicted deformation behavior of the 60 and 80 vol % Ni interpenetrating-phase composites calculated using Equation 12 and using the new constraint factor (Equation 13) is shown in Fig. 13. Note that the new model yields excellent agreement with the observed behavior of these composites.

As a final note, Tuan *et al.* [31] prepared fully dense Al_2O_3 composites with less than 13% Ni by pressureless sintering of coated powders. Increases in fracture strength of up to 23% were reported and attributed to matrix grain refinement. In this case, however, fracture stress typically exhibits an inverse square root dependence on grain size. Since grain size refinements of approximately 10% were reported, increases in fracture strength of only about 5% would be expected. Using the fracture model described above, an increase in fracture strength of approximately 30% can be expected

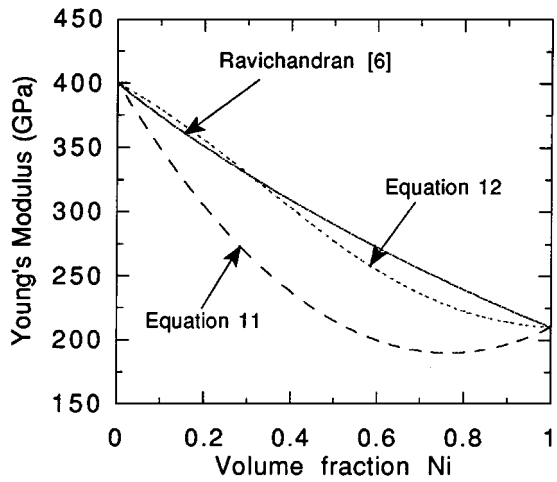

Figure 12 Dependence of Young's modulus on Ni content for interpenetrating-phase composites predicted using the model of Ravichandran [6], and the ROM deformation model with and without constraint (Equations 12 and 11, respectively).

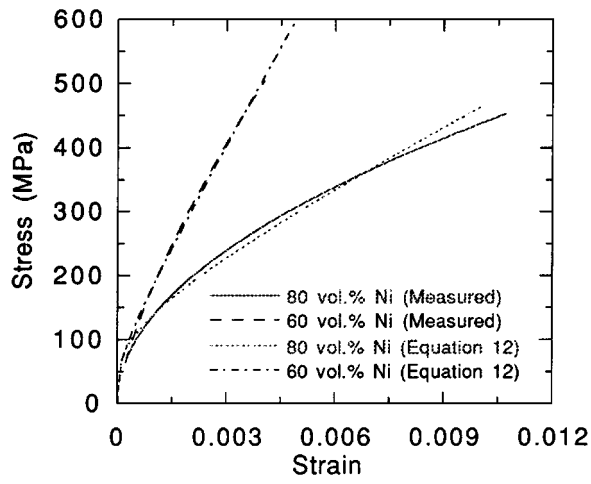

Figure 13 Deformation behavior of 60 and 80 vol % Ni composites compared with predictions using the ROM deformation model with constraint (Equation 12).

for thermal residual stresses on the order of 200 MPa. Although residual stress measurements were not reported, it is possible that the observed strength increases were due to the presence of residual stresses.

4. Conclusions

An effort has been made to employ simple ROM models in order to explain the deformation and fracture behavior of powder processed Ni-Al_2O_3 composites exhibiting a wide range of compositions and microstructures. For the purposes of these analyses, the materials were broadly classified as being particle-reinforced (either ceramic in metal matrix or metal in ceramic matrix) or having interpenetrating phases.

Ultrasonic elastic modulus measurements indicated that particle-reinforced composites with 20 vol % Ni and less had complete particle debonding, thereby exhibiting the elastic behavior of a porous ceramic. Particle-reinforced composites with between 40 and 60 vol % Ni exhibited elastic behavior indicative of materials containing substantial damage, which was attributed primarily to poor sinter bonding between contiguous Al_2O_3 particles. Both interpenetrating-phase and particle-reinforced composites of 80 vol % Ni, as well as the 60 vol % Ni with interpenetrating-phase exhibited elastic moduli consistent with ROM predictions.

Only Ni-Al_2O_3 composites containing 60 vol % Ni or greater exhibited significant inelastic deformation, which, in the case of the interpenetrating phase composites, was reasonably well modeled using ROM formulations. The 60 vol % Ni particle-reinforced composite was shown to contain significant damage that, when included in Ravichandran's ROM model, adequately explained the deformation behavior.

A new semi-empirical approach for predicting the fracture strain of continuous ceramic-matrix composites was presented based on porosity models. This approach successfully predicted the fracture strains of continuous ceramic-matrix composites containing 0 to 80 vol % Ni. Fracture stresses were calculated from fracture strains by treating the deformation behavior of these materials using a combined ROM and porous ceramic formulation. This new and simple model successfully predicted fracture stresses for all but the 60 vol % Ni composite. By using an empirical constraint factor to account for the interaction between the phases, this model successfully predicted the observed deformation behavior of 60 and 80 vol % Ni interpenetrating-phase composites.

With respect to modeling of FGMs, simple ROM-based models can be used to reasonably predict the deformation behavior of a wide range of elastic and ductile composites, provided that they do not contain substantial microstructural damage. The modified ROM formulation requires selection of the q parameter, which is ambiguously related to the microstructure. In contrast, Ravichandran's ROM-based models require knowledge of only the deformation behavior of each phase, and the volume fraction. For particle-reinforced composites containing substantial damage, Ravichandran's model can still be applied. In this paper, we included damage in Ravichandran's particle-reinforced model by treating the composite as two different particle-reinforced phases, one with completely damaged particles and one with completely undamaged particles.

References

1. R. L. WILLIAMSON, B. H. RABIN and J. T. DRAKE, *J. Appl. Phys.* **74**(2) (1993) 1310.
2. J. T. DRAKE, R. L. WILLIAMSON and B. H. RABIN, *ibid.* **74**(2) (1993) 1321.
3. A. KAWASAKI and R. WATANABE, *J. Japan Inst. Metals* **51**(6) (1987) 525.
4. A. E. GIANNAKOPOULOS, S. SURESH, M. FINOT and M. OLSSON, *Acta Metallurgica et Materialia* **43**(4) (1995) 1335.
5. B. PAUL, *Trans. Metall. Soc. AIME* (1960) 36.
6. K. RAVICHANDRAN, *Compos. Sci. Technol.* **52** (1994) 541.
7. Idem., *Acta Metallurgica et Materialia* **42**(4) (1994) 1113.
8. J. GURLAND, *Mater. Sci. Eng.* **40** (1979) 59.
9. S. ANKEM and H. MARGOLIN, *Metall. Trans.* **17A** (1986) 2209.
10. I. TAMURA, Y. TOMOTA and H. OZAWA, in Proceedings of the Third International Conference on Strength of Metals and Alloys (Institute of Metal and Iron and Steel, London, 1973) p. 611.
11. H. FISCHMEISTER and B. KARLSSON, *Z. Metallkde* **68**(5) (1977) 311 .
12. J. D. ESHELBY, *Proceedings of the Royal Society of London* **A241** (1957) 376.
13. J. W. HUTCHINSON, *Proceeding of the Royal Society* **A319** (1970) 247.
14. T. MORI and K. TANAKA, *Acta Metallurgica et Materialia* **21** (1973) 571.
15. K. TANAKA and T. MORI, *ibid.* **18** (1970) 931.
16. Y.-L. SHEN, M. FINOT, A. NEEDLEMAN and S. SURESH, *ibid.* **43**(4) (1995) 1701.
17. J. YANG, S. M. PICKARD, C. CADY, A. G. EVANS and R. MEHRABIAN, *ibid.* **39** (1991) 1863.
18. T. MOCHIDA, M. TAYA and M. OBATA, *JSME International Journal Series I* **34** (1991) 187.
19. W. TONG and G. RAVICHANDRAN, *Compos. Sci. Technol.* **52** (1994) 247.
20. R. L. COBLE and W. D. KINGERY, *J. Amer. Ceram. Soc.* **39** (1956) 381.
21. B. H. RABIN and R. J. HEAPS, *Ceram. Trans.* **34** (1993) 173.
22. D. STAUFFER and A. AHARONY, "Introduction to Percolation Theory" (Taylor & Francis, London, 1994) p. 91.
23. A. W. THOMPSON, *Acta Metallurgica et Materialia* **25** (1977) 83.
24. G. S. DAEHN, B. STARCK, L. XU, K. F. ELFISHAWY, J. RINGNALDA and H. L. FRASER, *ibid.* **44** (1996) 249.
25. R. M. GERMAN, "Powder Metallurgy Science" (Metal Powder Industries Federation, Princeton, New Jersey, 1984) p. 214.
26. J. C. JAEGER and N. G. W. COOK, "Fundamentals of Rock Mechanics" (John Wiley & Sons, New York, 1976) p. 225.
27. A. A. GRIFFITH, in Proceedings of the First International Congresson on Applied Mechanics (Delft, 1924) p. 55.
28. D. BROOKSBANK and K. W. ANDREWS, *Journal of the Iron and Steel Industry* (1969) 474.
29. *Idem., ibid.* (1972) 246.
30. X.-L. WANG, Oak Ridge National Engineering Laboratory, unpublished results.
31. W. H. TUAN, H. H. WU and T. J. YANG, *J. Mater. Sci.* **30** (1995) 855.

Received 2 January 1997
and accepted 7 October 1998